



Universiteit  
Leiden  
The Netherlands

## Development of novel anti-cancer strategies utilizing the zebrafish xenograft model

Chen, Q.

### Citation

Chen, Q. (2020, September 1). *Development of novel anti-cancer strategies utilizing the zebrafish xenograft model*. Retrieved from <https://hdl.handle.net/1887/136271>

Version: Publisher's Version

License: [Licence agreement concerning inclusion of doctoral thesis in the Institutional Repository of the University of Leiden](#)

Downloaded from: <https://hdl.handle.net/1887/136271>

**Note:** To cite this publication please use the final published version (if applicable).

Cover Page



Universiteit Leiden



The handle <http://hdl.handle.net/1887/136271> holds various files of this Leiden University dissertation.

**Author:** Chen, Q.

**Title:** Development of novel anti-cancer strategies utilizing the zebrafish xenograft model

**Issue Date:** 2020-09-01

# Chapter 2

## Lactic acid secreted by glycolytic B16.F10 melanoma cells attracts macrophages to drive angiogenesis

Quanchi Chen <sup>1</sup>, Xiaobing Zhang <sup>2</sup>, Daan Kloosterman <sup>1</sup>, Sylvia Le Dévédec <sup>2</sup>, B. Ewa Snaar-Jagalska <sup>1\*</sup>

1 Institute of Biology, Leiden University, Leiden, The Netherlands

2 Institute of Drug Discovery & Safety division, Leiden University, Leiden, The Netherlands

\* Correspondence: b.e.snaar-jagalska@biology.leidenuniv.nl; Tel.: +31-71-527-4980 (E.S.J.)

**Manuscript in preparation**

**Keywords:** melanoma, macrophages, angiogenesis, lactic acid, zebrafish xenograft

## Abstract

Malignant melanoma is often linked to increased angiogenesis and a high infiltration with tumor-associated macrophages (TAMs). TAMs influence various processes during tumor development, including immune responses, tumor growth, metastasis and angiogenesis. These immune cells may act as a local source of Vascular endothelial growth factor (VEGF), thereby stimulating neo-vascularization. However, the dynamic interactions between macrophages and the tumor environment, including melanoma and endothelial cells, remain elusive. We utilized a zebrafish allo- and xenograft model to understand the role of macrophages during melanoma progression and tumor-induced angiogenesis. Three red fluorescence-labeled melanoma cell lines (zebrafish ZMEL1, human SK-MEL28 and mouse B16.F10) were injected into transgenic reporter *Tg(mpeg:GAL4:UAS:lifeact:GFP)* embryos with green fluorescent macrophages to study the interaction between melanoma cells and host macrophages. First, we compared the interactions between xeno- and allografted melanoma cells with macrophages, to ensure the response is not due to cross-species immune recognition. Next, the recruitment of macrophages to the primary tumor was analyzed. Additionally, the functional significance of these immune cells was studied by chemical ablation of macrophages in *Tg(mpeg:GAL4:UAS:NTR:mCherry)* embryos, using metronidazole (MTZ). The growth kinetics and angiogenic activity of each engrafted cell line were quantified in the presence and absence of macrophages. Finally, the function of lactic acid secreted by glycolytic B16.F10 melanoma cells was investigated after chemical inhibition of glycolysis. We observed that macrophages are attracted to lactic acid, secreted by glycolytic B16.F10 cells and subsequently promote their angiogenic potential.

## Introduction

Cutaneous melanoma is an aggressive type of skin cancer which arises when pigment-producing skin cells, called melanocytes, become cancerous. Whereas healthy melanocytes respond properly to growth signals, melanoma cells proliferate, form blood vessels, invade the circulatory system and spread to distant tissues and organs. A high ability to metastasize makes melanoma one of the deadliest forms of cancers. Unfortunately, melanoma is becoming more common every year and is now the second most common cancer type in young people [1].

The progression of cutaneous melanoma can be defined by a multi-phase model, from benign nevus, dysplastic nevus, radial growth phase, to vertical growth phase and metastatic melanoma [2]. The key driver behind its development is the accumulation of mutations in crucial genes which regulate cell growth, differentiation and survival. Mutations are primarily due to prolonged ultra-violet radiation (UVR) exposure. In the benign nevus stage, oncogenic mutations in the BRAF and N-RAS genes pave the way for melanoma development. After acquiring these mutations, a dysplastic nevus is shaped, which is characterized by molecular abnormalities that affect cell growth, DNA repair and survival. In this stage, loss of function mutations in tumor suppressor genes CDKN2A or PTEN are crucial for initiating the highly proliferative radial growth phase (RGP) and, henceforth, the migratory vertical growth phase

(VGP) [3]. In the VGP, melanoma cells lose cell-cell contact and undergo epithelial to mesenchymal transition (EMT). Finally, vertical growth of the tumor through the basement membrane of the dermis is followed by periods of increased angiogenesis. As the tumor continues to expand into the dermis, the need for nutrients and oxygen increases. Through angiogenesis, the tumor stimulates the development of new blood vessels from existing ones. Additionally, these vessels provide a transportation route for nutrients and oxygen but also a route for the melanoma cells to the circulatory system [4]. Before homing of the disseminated melanoma cells (DMCs) at a secondary site, a pre-metastatic niche is formed as a result of the accumulation of lysosomal oxidase, placental growth factor (PIGF) and exosomes derived from the primary tumor. The pre-metastatic niche promotes metastatic colonization upon arrival of the DMCs [5]. The DMCs extravasate from the circulatory system into the tissue and begin to proliferate, resulting in the formation of a secondary tumor.

It is generally accepted that the tumor microenvironment (TME) is an important factor in tumorigenesis. The TME is highly heterogeneous and is composed of various cell types which can either enhance or inhibit tumor growth [6]. Among these are immune cells such as macrophages, neutrophils, natural killer cells and T cells. During development, cancers acquire hundreds or even thousands of mutations in coding exons, promoting the production of tumor specific- and tumor-associated proteins. These proteins, respectively, may serve as tumor-specific-antigens (TSAs) and tumor-associated-antigens (TAAs) for recognition by the immune system [7,8]. Upon recognition of these antigens, attracted immune cells provide immunosurveillance and destroy malignant cells [9].

In contrast, the host's immune system can also promote tumor survival, growth and metastasis [10]. Some malignant cells are able to secrete molecules which change the cellular composition and function of the TME, thereby evading immunosurveillance [11]. The established TME shares many similar features with a chronic wound, inducing a wound-healing-like immune response. When immune cells are recruited to the TME, they secrete inflammatory cytokines, growth factors and chemokines, which in turn stimulate tumor growth, angiogenesis and migration [12].

One of the most abundant immune cells in the melanoma TME are macrophages, which are characterized by their plasticity and flexibility. Owing to their plasticity, macrophages alter their phenotype continuously, following environmental cues and intercellular interactions [13]. Conventionally, macrophage phenotypes have been classified in two main groups, namely the pro-inflammatory type I macrophages (M1) and the anti-inflammatory type II macrophages (M2) [14]. However, these phenotypes should not be seen as binary, but as a spectrum where M1 and M2 macrophages are at the opposite end [15,16]. M1 polarization is promoted by pro-inflammatory stimuli such as interferon gamma (IFN $\gamma$ ), tumor necrosis factor alpha (TNF- $\alpha$ ) and toll-like receptor (TLRs) ligands. Many pro-inflammatory cytokines are secreted by M1 macrophages, including IL-1 $\beta$ , TNF- $\alpha$ , TNF- $\beta$  and IL-6. Whereas M1 macrophages are involved in the initial tissue damage response, M2 macrophages dominate later in repair [17,18]. Polarization towards an M2 phenotype is induced by IL-

4, IL-13, the immune complex or glucocorticoids. M2 macrophages are characterized by their secretion of TGF- $\beta$ , IL-10, VEGF and matrix metalloproteinases (MMPs), thereby assisting in the resolution of inflammation, and the promotion of tissue remodeling and repair [19].

Melanoma cells secrete several factors that attract monocytes, including lactic acid, VEGF, and colony-stimulating factor (CSF-1). Upon arrival at the tumor site, monocytes may differentiate into tumor-associated macrophages (TAMs). In cutaneous melanoma, TAMs exhibit heterogeneous responses which can be pro- and antitumoral. It has been found that the function and phenotype of macrophages changes during melanoma progression. During the early neoplastic phase, macrophages play a proinflammatory role and provide immune surveillance, whereas macrophages in a malignant melanoma environment can promote angiogenesis and enhance tumor cell dissemination [20,21]. Therefore, pharmacological targeting of the macrophage activity depends on the stage of the disease.

In melanoma, neovascularization is linked to high malignancy and metastasis, and is a crucial predictive factor in melanoma tumorigenesis [22]. Toriso H. et al. found that the number of infiltrating macrophages and blood vessels positively correlated with the depth of melanoma invasion. They suggest that activated macrophages are a local source of VEGF and that these immune cells upregulate pro-angiogenic factors IL-8 and VEGF in melanoma cells through secreting TNF- $\alpha$  and IL-1 $\beta$  [23]. How activated macrophages dynamically interact with melanoma cells and vascular endothelial cells remains unknown. However, using zebrafish as a model organism makes it possible to study these dynamic interactions *in vivo*. Over the last decade, zebrafish have emerged as a convenient *in vivo* model for cancer, immune and stem cell research. More than 70% of all human disease genes have a functional homolog in zebrafish [24]. Another advantage of this model is breeding efficiency. One zebrafish pair can produce up to 200 embryos per week, which develop *ex vivo* and are transparent, making them easy to study [25]. Additionally, the adaptive immune system is absent in early stage embryos, allowing tolerance for human tumor cell engraftment and exclusive study of the innate immune system [26]. In this research we aimed to microscopically trace macrophages in an allo- and xenograft zebrafish models and dissect their role in the tumor induced angiogenesis. The transgenic line, *Tg(kdlr:GFP/mpeg:NTR:mCherry)* with fluorescent blood vessels (green) and macrophages (red) was employed here to study the interaction between macrophages, vessels and engrafted melanoma cells (red and far red). Importantly, this transgenic line made possible to deplete macrophages in live embryos in the inducible fashion by adding metronidazol (MTZ) to the medium, which in turn was broken down by nitroreductase (NTR) enzyme to toxic compound, ablating macrophages [27]. Melanoma cells were engrafted into the Duct in Cuvier (DOC) or within the perivital space of two days old embryos, where they settled, formed a primary tumor and induced angiogenesis. Using these models, we observed attraction of macrophages to engrafted melanoma cells of different origin. Restrictively, macrophages attracted to lactic acid, secreted by glycolytic B16.F10 cells elevated their angiogenic response.

## Methods

### Transgenic Fish Lines

The transgenic lines *Tg(kdlr:GFP/mpeg:NTR:mCherry)* and *Tg(mpeg:GAL4:UAS:lifect:GFP)* were used in this study and were handled in compliance with local animal welfare regulations and maintained according to standard protocols ([www.ZFIN.org](http://www.ZFIN.org)). Zebrafish embryos were collected and treated with 0.2 mM *N*-phenylthiourea at 24 hours post fertilization (hpf) to prevent melanization. To deplete macrophages, *Tg(mpeg:GAL4:UAS:NTR:mCherry)* fish were exposed to 2.5 mM metronidazol (MTZ) at 48 hpf. The medium of 2.5 mM MTZ treated embryos was refreshed every two days.

### Melanoma Cell Lines

Cell lines ZMEL1, a zebrafish melanoma cell line, kindly provided by dr. Richard M. White [28], SK-MEL28, a human- cutaneous melanoma cell line, and B16.F10, a mouse melanoma cell line from the ATTC, were used. The cell lines were cultured in DMEM/F12 10% Fetal Calf Serum (FBS; Gibco). Stable fluorescent cell lines were created using lentiviral vectors expressing GFP or far red.

### Cell proliferation assay

Sulforhodamine B (SRB) colorimetric assay was used to evaluate cell proliferation as described previously [29]. B16.F10 cells were seeded in a 96-well plate and left overnight. Cells were treated with different doses of 2-Deoxyglucose (2DG) for different times as indicated and then were fixed with 30  $\mu$ L 50% trichloroacetic acid (TCA, Sigma-Aldrich) for 1 h at 4 °C. Cellular proteins were stained with 60  $\mu$ L 0.4% SRB (Sigma-Aldrich) for 30 min and unbound SRB was removed by washing with 1% acetic acid 5 times (VWR, Amsterdam, The Netherlands). Protein-bound SRB was dissolved in 200  $\mu$ L 10 mM unbuffered Tris (Thermo Fisher) and solution absorbance was measured at 540 nm on an Infinite M1000 microplate reader (Tecan, Giessen, The Netherlands). Dose response curves and IC50 values were made in GraphPad Prism (version 8.1.1).

### ATP luciferase assay

Following the manual's instructions of the ATPlite 1 step Kit (PerkinElmer, the Netherlands), optimized number of cells were seeded on the black screen-star plate (Greiner, the Netherlands) and attached overnight in the incubator. After staining with Cells Hoechst for 45 mins, cells were treated with exposure medium. Prior to assay, the images of nuclei were captured on a Nikon Eclipse Ti microscope using a Plan Fluor 10 objective with 37 °C 5% CO<sub>2</sub> incubator chamber, automated stage and perfect focus. At indicated measurement time, each plate well was replaced with 50  $\mu$ L fresh medium and then 50  $\mu$ L of ATP substrate was added. After 2 mins mixture on the shaker, luminescence was measured with FLUO star plate reader (BMG Labtech, the Netherlands). All graphs were plotted in Graphpad Prism. The numbers of cells were calculated by custom-made ImagePro macro. All values were normalized to cell numbers.

### **Lactate assay**

Cells were cultured and treated with 100  $\mu$ L indicated compound medium in 96 well plate. At collection time, cells were removed by spinning down and supernatants were collected to a new 96-well plate. 10  $\mu$ L of supernatant was mixed with ... of lactate assay reagent (including 108 mM Triethanolamine HCl, 10.7 mM EDTA.Na<sub>2</sub>, 42 mM MgCl<sub>2</sub>). After 7 mins incubation in the dark, absorbance was measured at wavelength of 490 nm on FLUO star plate reader (BMG Labtech, the Netherlands). Meantime, cells were stained with Hoechst and the images of nuclei were captured on a Nikon Eclipse Ti microscope using a Plan Fluor 10 objective with 37 °C 5% CO<sub>2</sub> incubator chamber, automated stage and perfect focus. All graphs were plotted in Graphpad Prism. The numbers of cells were calculated by custom-made ImagePro macro. All values were normalized to cell numbers.

### **Embryo Preparation and Tumor Injection**

Zebrafish embryos at 2 days post fertilization (dpf) were anaesthetized with tricaine and translocated to a Petri dish coated with 1% agarose. Melanoma cells were trypsinized and collected as a single cell suspension in a 15ml collection tube. After 5 minutes centrifuging at 1200 rpm the supernatant was removed and the pellet was resuspended in phosphate-buffered saline (PBS). After second centrifugation the supernatant was removed, pellet was resuspended in 10 $\mu$ l 2% PVP and kept at room temperature before implantation. The cell suspension was transferred into glass capillary needles (nr 99.) and the injections were performed with a Pneumatic Pico pump with a manipulator (WPI) within 2 hours. ~50 ZMEL1 cells, ~300 SK-MEL28 or ~300 B16.F10 cells were injected above the ventral end of the Duct of Cuvier or within the perivital space [30,31]. As a negative control, 2% PVP was injected instead. ZMEL1 injected fish were maintained at 28°C, whereas SK-MEL28 and B16.F10 injected fish were kept at 34°C.

### **Macrophages attraction assay**

1 nL of purified CCL<sub>2</sub> protein (R&D Systems, The Netherlands) or lactic acid (Sigma Aldrich, The Netherlands) (10 ng/ml) were injected into the hindbrain ventricle of *Tg(kdlr:GFP/mpeg:NTR:mCherry)* larvae at 48 hpf [32]. 1 nL of PBS injected embryos were set as an injected control group. Samples were fixed with 4% PFA at 3 hours post injection (hpi), and macrophages were counted within the hindbrain ventricle under a Zeiss Observer 6.5.32 laser scanning confocal microscope (Carl Zeiss) by going through the z-stacks, comprising the whole hindbrain ventricle.

### **Microscopy and Analysis**

Before confocal live imaging, larvae were anaesthetized with tricaine and positioned on a glass cover plate before embedding them in 0.5% low melting agarose. The position of larvae was corrected after embedding with a toothpick to obtain a uniform view of all samples for confocal imaging. For stereo live imaging, anaesthetized larvae were positioned on a 1% agarose covered Petri dish. After stereo imaging, embryos were translocated to a 48-wells plate, and were subjected to confocal imaging to

monitor tumor growth in each embryo at higher magnification. A Leica TCS SPE confocal microscope and a Leica stereo microscope were used to acquire fluorescent images. Time-lapse movies and three-dimensional images were reconstructed using ImageJ. The stereo *xy* and confocal *xyz* images were analyzed in ImageJ. The data generated in ImageJ was transferred to excel and Prism 6 software (GraphPad) for further analysis.

### **Statistical Analysis**

The statistical analysis was performed using Prism 6 software. Comparisons between two groups were calculated with one-tailed non-parametric unpaired t-tests. Comparisons between more than two groups were performed with a multi-way ANOVA. Not significant ( $p > 0.05$ ), \* $0.01 < p < 0.05$ , \*\* $0.001 < p < 0.01$ , \*\*\*  $p < 0.001$ .

### **Results**

#### **Zebrafish model to study melanoma growth and angiogenesis formation**

To study the interactions between macrophages and melanoma cells, we took advantage of the allo- and xenograft zebrafish model. Injecting fluorescence-labeled tumor cells into the Duct of Cuvier (DOC) of two-day old transgenic embryos allowed us to follow the growth kinetics of these cells in the presence of a microenvironment [30]. The head and tail, representing the primary tumor and the extravasation site, respectively, were imaged at various time points (Figure 1A). We tested three melanoma cell lines with BRAF<sup>V600E</sup> and p53<sup>-/-</sup> mutations, including zebrafish melanoma cell line ZMEL1, human cutaneous melanoma cell line SK-MEL28 and mouse melanoma cell line B16.F10. The number of melanoma cells that were injected was optimized by taking into account the survival of the embryos and tumor cells. We found that all cell lines formed a tumor at the injection site and migrated to the caudal hematopoietic tissue (CHT) (Figure 1B). ZMEL1 cells were highly proliferative at the injection site and formed a solid primary tumor surrounding the skin of the embryo at 6dpi. These cells showed low single cell extravasation from the vessel at the CHT without establishing a secondary tumor in the tail fin. We found that SK-MEL28 cells induced high extravasation and were more invasive, however they did not establish a solid primary tumor at the injection site. In contrast, these cells did form a secondary tumor at the CHT. B16.F10 cells induced a compact primary tumor on the skin, induced angiogenesis and established a secondary tumor, while SK-MEL28 induced a primary tumor without clear angiogenesis (Figure 2C). All cell lines were able to form primary tumors in the embryos, which allowed us to study the role of macrophages during the tumor growth of these cell lines after transplantation.

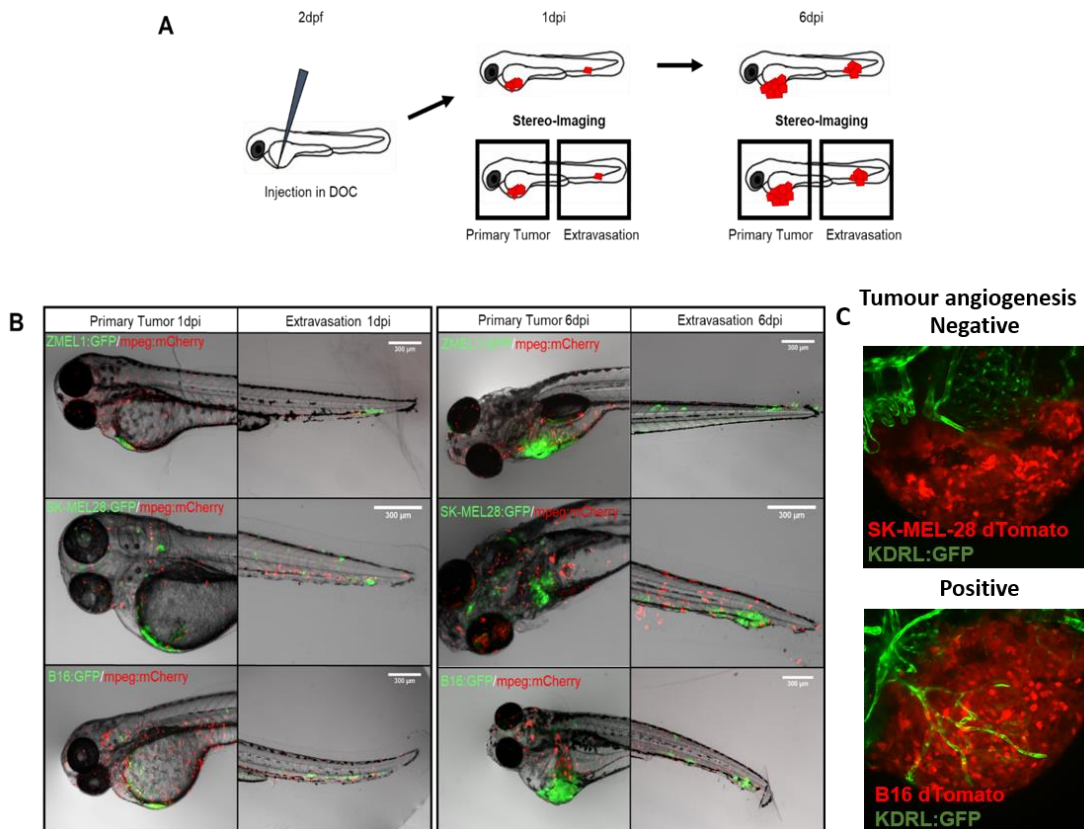


Figure 1 Experimental setup and melanoma growth dynamics in zebrafish embryos. An allo- and xenograft zebrafish model was used to study the role of macrophages on engrafted melanoma development. Around 300 tumor cells were injected into the Duct of Cuvier at 2 dpf. After injection of fluorescence-labeled tumor cells in the DOC, stereo and confocal images were taken at various time points of the head and tail respectively (A). Representative images show the ZMEL1, SK-MEL28 and B16.F10 primary tumor site and extravasation. The mCherry labeled macrophages are located throughout the entire embryo (B). Negative tumor angiogenesis formation (SK-MEL-28) and positive tumor angiogenesis formation (B16) at the primary site (C).

### Host macrophages recruited to injection site and interact with engrafted melanoma cells

We next asked if host macrophages respond to engrafting of melanoma cells and whether interaction occurs between these cells. Injecting dTomato-labeled tumor cells into transgenic embryos with GFP-labeled macrophages allowed us to trace the migration and behavior of the tumor cells and macrophages for 10 hpi by using time lapse imaging (Figure 2A). The mock injection procedure induced accumulation of macrophages near the injection site. The macrophage population surrounding the 2% PVP injection resolved between 3-6hpi, indicating a resolution of inflammation. However, the macrophage population at the tumor injection site remained high and gradually increased until the termination of the experiment, suggesting that macrophages are attracted to the primary tumor and not the injection wound (Figure 2B). To ensure that there were close interactions between these cells, we reconstructed three-dimensional images of confocal z-stacks from the primary tumor. These images reveal that macrophages interacted closely with tumor cells and quickly infiltrated the engrafted tumor (Figure 2C).

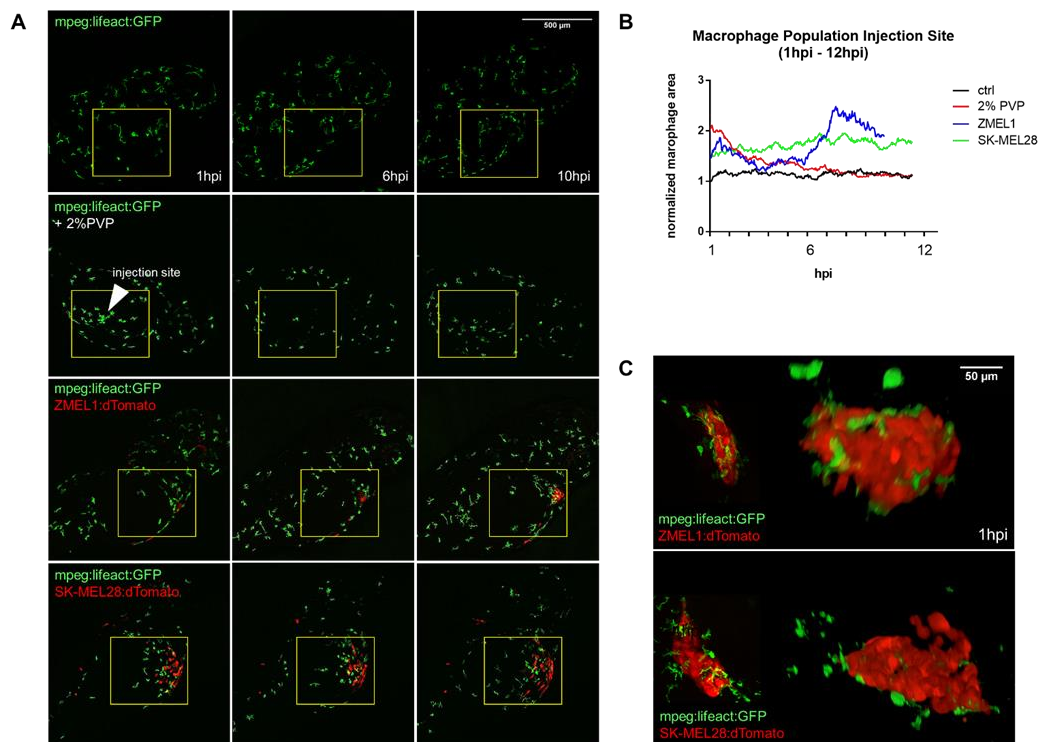


Figure 2 Tracking macrophage migration and their interactions with melanoma cells. Still images from the time lapse at 1hpi, 6hpi and 10hpi. Each row represents a single embryo, either non-injected or injected with 2% PVP, ZMEL1 or SK-MEL28. Images were taken with a 10x magnification. Macrophages accumulated near the injection site, which is marked in yellow (A). Quantification of the macrophage area at the injection site of each frame within the time lapse. A 175x175 pixels ROI was used to represent the injection site. The fluorescent signal in this ROI was normalized by dividing it by the total fluorescent expression in the same channel. Macrophages quickly respond to the injection, but only continued to accumulate near the injection site when tumor cells were present (B). 2D/3D reconstructed confocal z-stacks of the ZMEL1 and SK-MEL28 primary tumor at 1hpi, obtained with a 40x magnification. Right, the 3D image is shown of the 2D images, which is visualized on the left. Macrophages infiltrated the engrafted tumor at 1hpi (C).

### Macrophages continue to accumulate at the primary tumor site

To verify whether engrafted melanoma cells continue to recruit macrophages during the timespan of our experiments, we analyzed and quantified three-dimensional images of the primary tumor at 1hpi, 1dpi and 4dpi (Figure 3A). At 1hpi and 1dpi, SK-MEL28 had a significantly-larger tumor area than ZMEL1. However, ZMEL1 showed a trend to have a larger tumor area at 4dpi compared to SK-MEL28, suggesting that ZMEL1 proliferated more effectively. The number of macrophages in the field of view (FOV) of the injection site was similar between 2% PVP and tumor-injected embryos at 1hpi. The number of macrophages in the FOV of the primary tumor induced by ZMEL1 and SK-MEL28 injection gradually increased at 1dpi and 4dpi, whereas the population of macrophages at the 2% PVP injection site remained constantly small throughout the experiment (Figure 3B and 3C). The macrophages in proximity of the tumor showed a more rounded morphology, characterizing an inflammatory

phenotype. Occasionally, macrophages and melanoma cells showed overlap between their fluorescence signal, indicating that macrophages phagocytose tumor cells or debris (Figure 3D). These results suggest that macrophages are recruited to the engrafted tumor throughout and that these cells continuously interact with one another during the timespan of our experiments.

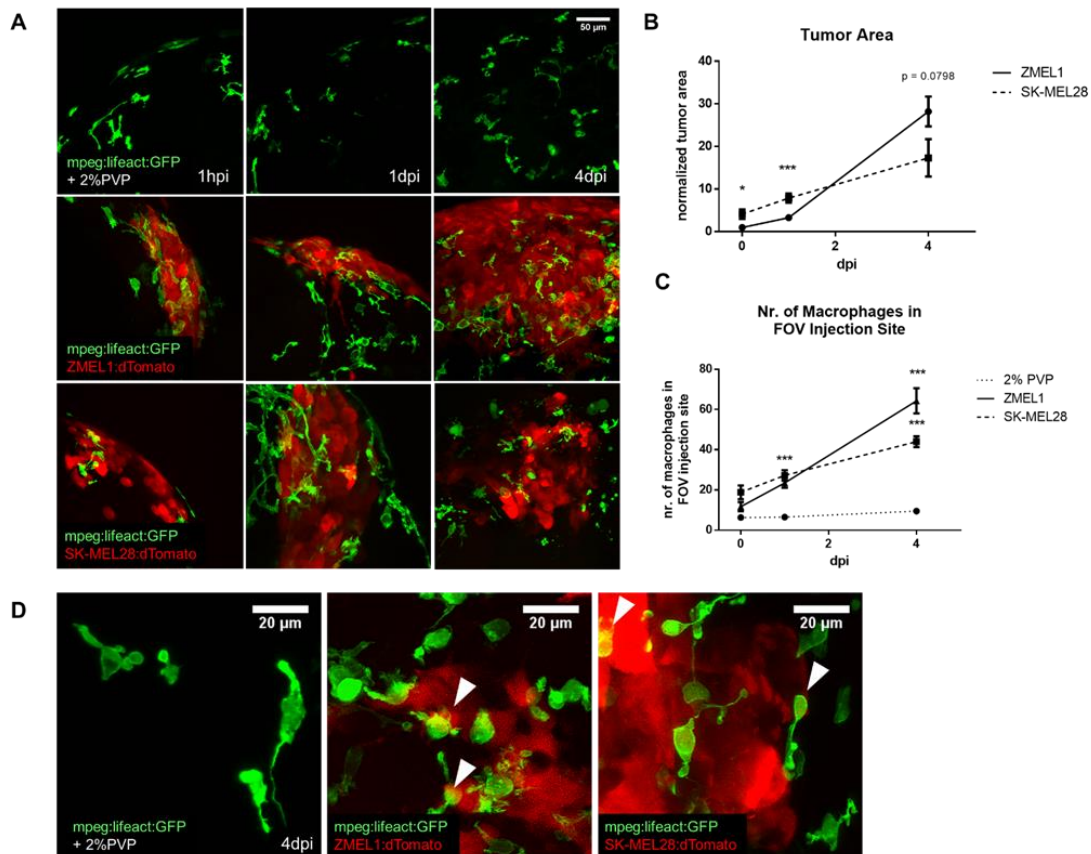


Figure 3 Macrophages accumulate at the primary tumor site. Representative confocal images from the injection site of 2% PVP, ZMEL1 and SK-MEL28 injected embryos at 1hpi, 1dpi and 4dpi, obtained with a 40x magnification. Macrophages are labelled with lifect:GFP and melanoma cells with dTomato (A). Quantification of the area of the ZMEL1 and SK-MEL28 primary tumor. The tumor area represents the z-stacked 2D area of each tumor. Each data point represents the average area at that time point. The error bars represent the  $\pm$  SD. Non-parametric unpaired t-test was performed between each group (B). Quantification of the number of macrophages in the field of view (FOV) of the 2% PVP, ZMEL1 and SK-MEL28 injection site. An object larger than 10.000 voxels within the field of view (FOV) of the injection site was identified as a macrophage. Each point represents an average of 10 observations (n=10) and the error bars correspond to the mean  $\pm$  SD. Non-parametric unpaired t-test was performed between each group. The number of macrophages gradually increased at the tumor site (3C). The characteristic morphology of macrophages at 4dpi under different circumstances was imaged. The macrophages outside tumor were more elongated, directional comparing to rounded macrophages inside the tumor. The white arrows mark macrophages phagocytose tumor cells (3D).

### Metronidazol (MTZ) effectively depletes macrophages in *Tg(mpeg:GAL4:UAS:NTR:mCherry)* embryos

To study the functional significance of macrophages during melanoma development, we utilized the NTR/MTZ ablation system to deplete macrophages [33,34]. Embryos from 2dpf until 8dpf were exposed to various concentrations of MTZ to optimize the efficiency of the macrophage's ablation without sign of toxicity. We observed that all MTZ concentrations successfully depleted macrophages in embryos from 3dpf until the termination of the experiment at 8dpf (Figure 4A). Furthermore, treatment with 2.5mM, 5mM and 7.5mM MTZ had no effect on the survival of embryos. Embryos treated with 10mM MTZ showed enhanced lethality, indicating that MTZ is toxic at higher concentrations (Figure 4B). Increasing the concentration affected the development of the embryos, as embryos treated with a higher concentration were significantly shorter (Figure 4C). Based on these findings, a concentration of 2.5mM MTZ was used throughout this study to successfully deplete macrophages.

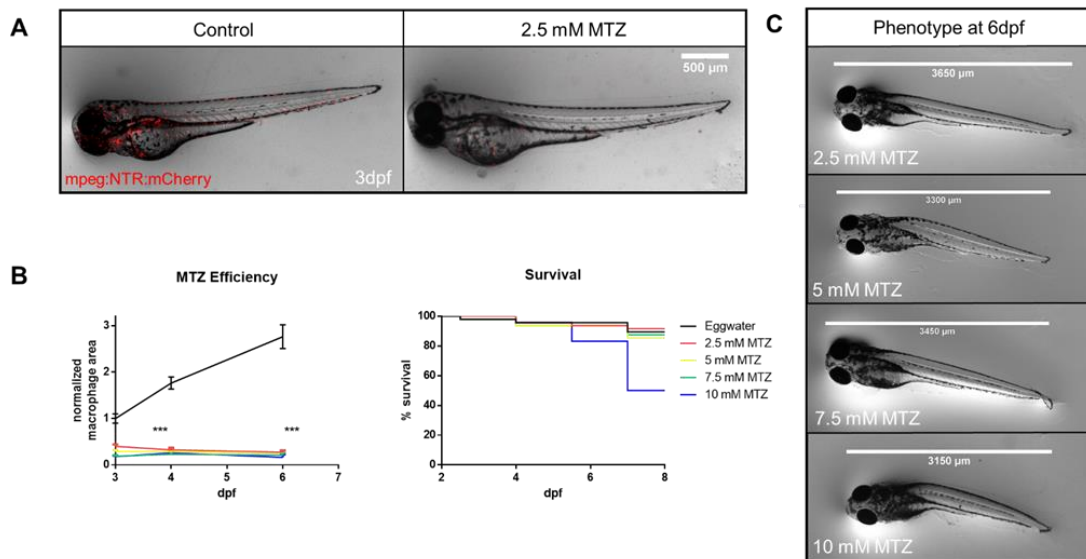


Figure 4 Efficiency and toxicity of NTR/MTZ Ablation System. We treated *Tg(mpeg:NTR:mCherry)* embryos with MTZ at 2dpf to deplete macrophages. Representative images of the macrophage population of untreated and 2.5mM MTZ treated embryos at 3dpf. Macrophages are labeled in mCherry (A). The macrophage area and survival rate of various treatments, including 2.5mM, 5mM, 7.5mM and 10mM were quantified. MTZ successfully depletes macrophages and is lethal at a concentration of 10mM (B). The effect of different MTZ concentrations on the length of the embryos. Increasing the concentration negatively correlated with the embryo length (C).

### B16.F10 ells rely on macrophages for tumor angiogenesis

As macrophages are known to be crucial in angiogenesis, we asked whether macrophage depletion indirectly inhibits primary tumor growth through impairing neo-angiogenesis. To investigate the effect of macrophage ablation on vascularization induction by each engrafted cell line, we imaged the primary tumor and their vascular network at various time points in *Tg(kdlr:GFP/mpeg:NTR:mCherry)* embryos in the presence and absence of macrophages. After injection in the DOC, ZMEL1 and B16.F10 formed solid tumors at 6dpi. In line with previous data, SK-MEL28 cells formed no solid tumor, but invaded the

tissue where blood vessels were already located (Figure 5A). The neo-angiogenesis was quantified by calculating the percentage of embryos with a positive phenotype, which is characterized by having a solid primary tumor with a neo-vascular network. All SK-MEL28 injected embryos had a negative phenotype, as SK-MEL28 cells were unable to form a solid primary tumor. At 3dpi, all B16.F10 primary tumors induced neo-vascularization, whereas only 40% of ZMEL1 injected embryos had a positive phenotype. At 6dpi, B16.F10 had a higher percentage of neo-vascularized tumors compared to ZMEL1. We observed that macrophage ablation by MTZ severely lowered the percentage of neo-vascularized B16.F10 tumors at both timepoints. However, the percentage of positive phenotype of ZMEL1 injected embryos was not affected by macrophage depletion (Figure 5B). This data implies that B16.F10 angiogenesis is macrophage dependent, while ZMEL1 cells initiate angiogenesis in the absence of macrophages (Figure 5B-D).

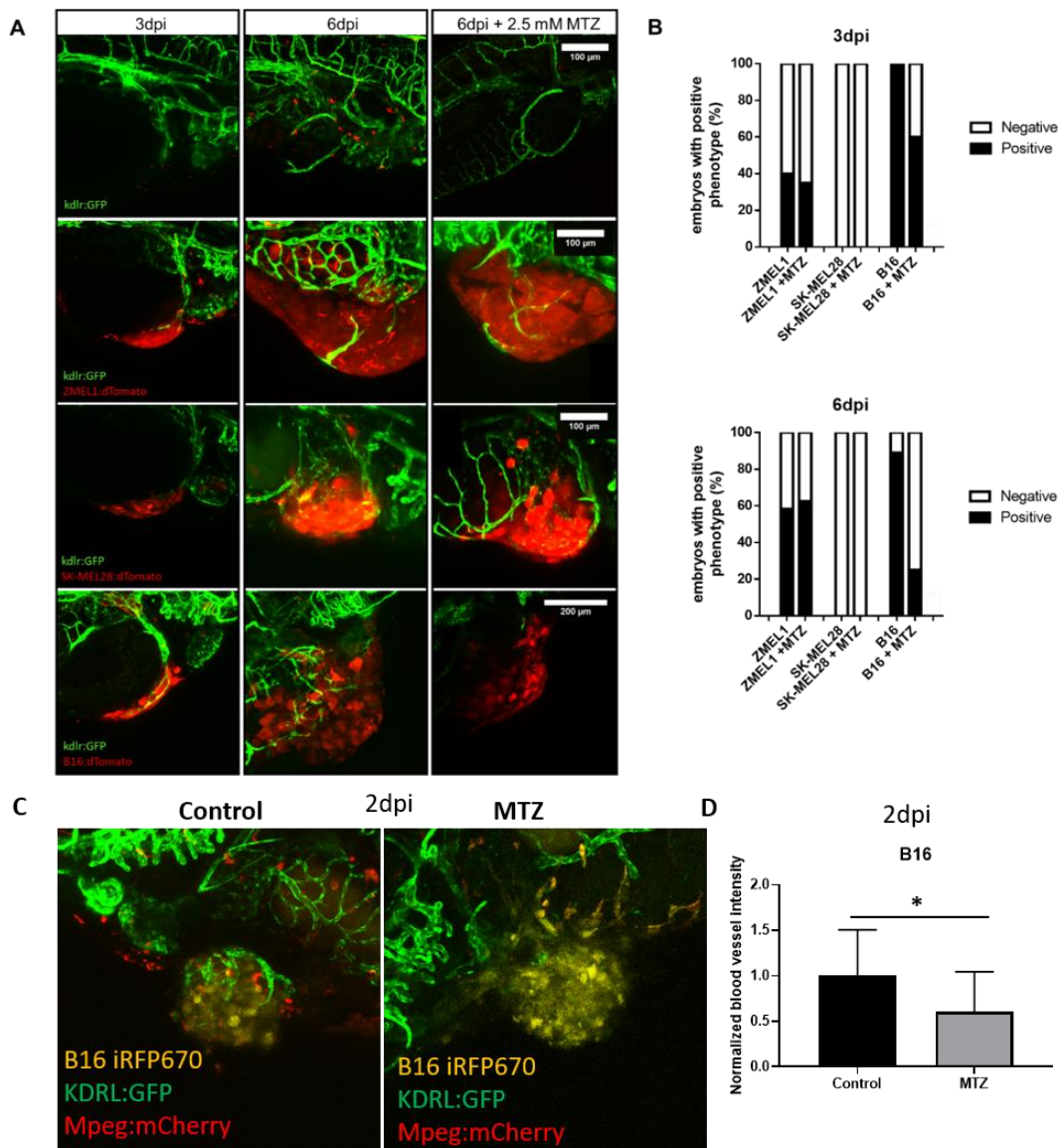


Figure 5 B16.F10 primary tumor relies on macrophages for neo-vascularization. The angiogenesis of the primary tumor was visualized to investigate the effect of macrophage depletion on the vascular network. Representative images are shown of each group at 3dpi and 6dpi, and 6dpi in combination with 2.5mM MTZ treatment (n=10).

The control group, *kdlr:GFP*, represents the vascular network in the absence of melanoma engraftment (A). The percentage of embryos with a solid primary tumor with a neo-vascular network. B16.F10 had the highest angiogenic activity. SK-MEL28 did not form a solid tumor, but invaded the surrounding tissue and nearby blood vessels. ZMEL1 neo-angiogenesis was not affected by macrophages depletion, whereas ablation of macrophages did inhibit neo-angiogenesis in B16.F10 primary tumors (B). Unfortunately, in the images depicted in B we are not able to distinguish macrophages from cancer cells as there were both labelled with red fluorescent marker, therefore we additionally conducted three colour experiments to confirm these results, using B16 iRFP670 cells expressing far- red fluorescence (C). The analysis was done by normalizing the blood vessel fluorescent intensity by tumor size at 2 dpi (D).

### **Angiogenic activity of B16.F10 is macrophage dependent**

To further prove that B16.F10 induced angiogenesis is macrophage dependent, we performed another *in vivo* angiogenesis assay, which is used to measure the angiogenic activity of tumor cells in 18hpi [31]. In this assay, the growth of the blood vessels from the sub-intestinal vein plexus (SIV) is analyzed in the presence of tumor cells. Angiogenic cells are able to induce sprouting or remodel the SIV complex [31]. ZMEL1, SK-MEL28 and B16.F10 cells were injected in the perivitelline space of 48hpf *Tg(kdlr:GFP/mpeg:NTR:mCherry)* and macrophage-depleted embryos. Growth of the blood vessels from the sub-intestinal vein (SIV) was imaged at 1 dpi (Figure 6A). The percentage of positive SIV phenotypes, which is characterized by tumor induced sprouting or complete remodeling of the complex, was calculated for each cell line. B16.F10 had the highest percentage of positive phenotypes, followed by SK-MEL28 and thereafter ZMEL1. Injection of 2% PVP induced no sprouting. The number of positive phenotypes induced by B16.F10 cells was severely decreased in macrophage depleted embryos (Figure 6B, 6C). The elongation of the SIV was quantified by dividing the length of the SIV by the width of the SIV. This parameter gives information about the attraction and sprouting of the SIV, as both increase the length of the SIV. B16.F10 significantly enhanced elongation of the SIV complex, whereas ZMEL1 and SK-MEL28 did not. Macrophage ablation significantly reduced the B16.F10 induced elongated phenotype of the SIV complex (Figure 6D). Additionally, we found that macrophage depletion overall inhibited the formation of the SIV complex, implying that macrophages are essential in the establishment of this complex (Figure 6E). In conclusion, these results suggest that B16.F10 has the highest angiogenic activity and that this activity is macrophage dependent.

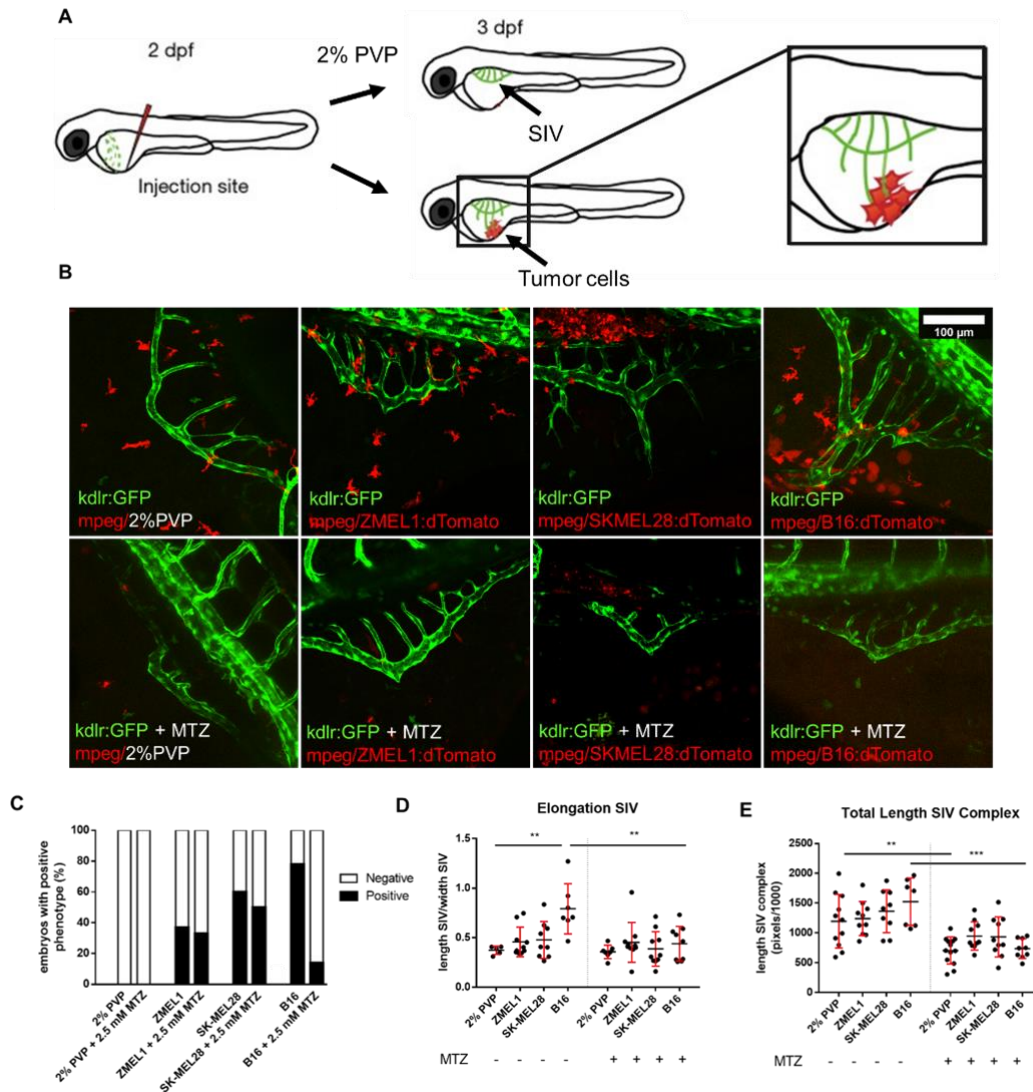


Figure 6 Macrophage ablation inhibits tumor-induced angiogenesis. An angiogenesis assay was performed to study the angiogenic activity of tumor cells. Tumor cells were injected in the perivitelline space of two-days old *Tg(kdlr:GFP/mpeg:NTR:mCherry)* embryos. 2% PVP was injected as a negative control. The SIV complex was imaged between 24-30hpi (A). Representative images of each injection and treatment groups. Blood vessels are labelled with GFP, macrophages and tumor cells lines with mCherry and dTomato therefore in these images we are not able to distinguish macrophages from cancer cells as there both are labelled with red fluorescent markers (B). The percentage of embryos with a positive phenotype, which is characterized by either attraction of the SIV or the formation of sprouts (C). Quantification angiogenic capability of tumor cells with (- MTZ) and without macrophages (+ MTZ). The elongation of the SIV complex was calculated by dividing the length by the width of the SIV complex. B16.F10, not ZMEL1 and SK-MEL28, induced elongation of the SIV complex towards the tumor, which was partly rescued through macrophage depletion (D). The total length of the SIV complex represents the total pixels of the skeletonized SIV complex. The error bars represent the standard error of each group (n=10). Macrophage depletion impaired SIV development in the presence of the tumor (E).

### **Lactic acid secreted by B16.F10 melanoma cells recruit macrophages to drive angiogenesis**

To address why macrophages are attracted to the tumor induced by engraftment of high glycolytic B16.F10 cells, we tested if lactic acid, product of glycolysis can attract macrophages in zebrafish model [35]. The lactic acid (10  $\mu$ M) was injected into the zebrafish hindbrain at 2 dpf, which is free of macrophages at this developmental stage (Figure 7A). As positive control we used human cytokine hCCL2, as well known chemoattractant of macrophages in zebrafish [36]. To estimate macrophages response to the local inflammation generated by wound we injected PVP solvent and compared to un injected control (Figure 7B). At 3hpi, the number of macrophages inside hindbrain was imaged and quantified (Figure 7B). Injection of hCCL2 and lactic acid significantly increased number of accumulated macrophages in the hindbrain comparing to number of macrophages in the same area of control and PVP injected embryos (Figure 7C). In order to verify if lactic acid is secreted by tumor cells to attract macrophages, B16.F10 cells were pre-treated with glycolysis inhibitor 2-deoxyglucose (2DG). The 24h treatment of cells with 10 mM 2DG sufficiently inhibited lactic acid secretion, without influencing cell proliferation and cellular ATP production (Figure 7D). After 24h of 10 mM 2DG treatment, around 300 far-red B16 cells were injected into DOC of 2 dpf embryos. Tumor size, macrophages infiltration, and blood vessels density inside tumor were analyzed at 2 dpi. The relative tumor area in 2DG group was not statistically reduced comparing to control group (Figure 7E). The fluorescence of macrophages and blood vessels was normalized by fluorescent tumor area in corresponding embryos and revealed that 2DG treatment impaired the macrophages accumulation and blood vessel intensity (Figure 7F) suggesting that indeed lactic acid secreted by B16.F10 cells contributes to macrophages accumulation and tumor blood vessels formation in zebrafish xenograft model.

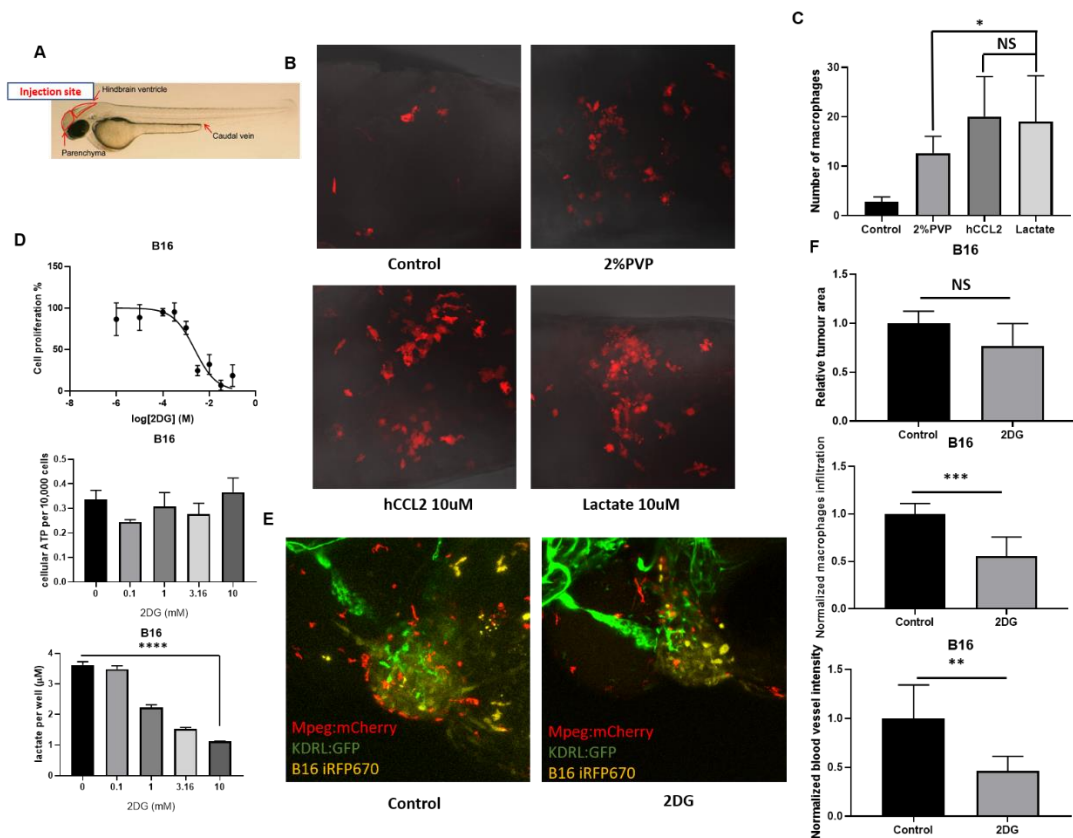


Figure 9 Lactic acid inhibition by 2DG in B16 tumor cells impairs macrophages accumulation and tumor angiogenesis formation. The macrophages attraction assay was performed here. 1 nL of lactic acid (10  $\mu$ M), 2% PVP and hCCL2 (negative and positive controls) were injected into hindbrain of zebrafish at 2 dpf (A). After 3h, the images of macrophages in the hindbrain were taken by fluorescent microscope (B). The number of macrophages was calculated (C). B16 cells were treated with 2DG (0.1, 2, 3.16, 10 mM) for 24 h. After treatment, the cell proliferation, cellular ATP per 10000 cells and lactate per well were measured (D). Around 300 B16 cells treated with 10 mM 2DG for 24 h were injected into Duct of Cuvier of 2dpf embryos. After 2 dpi, the fluorescent images were taken (E) and relative tumor area, normalized macrophages infiltration and normalized blood vessel intensity were quantified (E, F).

## Discussion

The malignancy of melanoma is often linked to increased angiogenesis and a high number of infiltrating TAMs [22,23]. Currently, many studies are aimed to understand the interplay between TAMs, melanoma and endothelial cells. However, the majority of these studies are conducted *in vitro* or *in vivo* using mouse models, which require complicated and invasive procedures to visualize dynamic interactions between tumor cells and their microenvironment. In contrast, the zebrafish xenograft model is a powerful platform to investigate dynamic cellular interactions within the tumor microenvironment, due to its transparency [25]. Injecting fluorescently labeled tumor cells into transgenic embryos with mCherry labeled macrophages allows us to study their interactions and behavior. In this work, we elucidated the functional significance of macrophages in primary tumor growth and neo-angiogenesis. We provided evidence that macrophages can enhance melanoma

growth by promoting neo-angiogenesis. Thus, we put forth a model which serves as the foundation for further research aimed to discover the exact molecular mechanism by which macrophages enhance neo-angiogenesis in melanoma, and thereby contribute to its malignancy. Initially, we asked if macrophages interact and respond to engrafted tumor cells. Through time lapse imaging and confocal analysis of the primary tumor, we found no differences between the first response of macrophages to 2%PVP and tumor injections. Within six hours, we observed a gradual decrease of macrophages surrounding the 2% PVP injection site, which suggests that resolution of inflammation occurred after the wound was repaired. Inflammatory responses associated with wound healing and tumors are remarkably similar. Tumors have been found to behave as wounds that do not heal, in order to establish a favorable microenvironment [37]. Accordingly, in the presence of melanoma cells, no resolution phase was observed. Additionally, macrophages continued to accumulate at the primary tumor until four days after injection. These results suggest that the engrafted melanoma cells continuously induce an inflammatory response, thereby recruiting macrophages. This response was not simply due to cross-species immune recognition, as we observed similar inflammatory responses towards allografted zebrafish ZMEL1 and xenografted human SK-MEL28 cells. The tumor fluorescent signals in macrophages suggest that these immune cells phagocytose components of the tumor. These components could be from alive tumor cells or from debris from dead tumor cells, as a result of phagocytosis. To further evaluate the function of macrophages during primary tumor growth, we depleted the entire macrophage population in embryos by utilizing the MTZ/NTR ablation system [33,34].

By comparing the growth kinetics of various melanoma cell lines in normal and macrophage depleted embryos, we found that macrophages promoted murine B16.F10 primary tumor growth, while inhibiting this process in ZMEL1 and SK-MEL28 tumors. We do not ignore the fact that macrophages could perform an anti-tumoral role during B16.F10 development at 6dpi. Hence, this could explain the marginal effect of macrophage depletion, as both the positive and negative functions of macrophages are abolished. The origin of each cell line was studied to find an explanation for the cell line dependent effect of macrophage depletion. The ZMEL1 cell line was obtained by Heilman S. et al. by harvesting *in situ* melanoma from transgenic *mitfa*-*BRAF*<sup>V600E</sup>; *p53*<sup>-/-</sup> zebrafish [38]. ZMEL1 cells are known to take advantage of the growth-promoting effect of the embryonic microenvironment, since these cells and the recipient are of the same species [28,39]. The xenografted cell line, SK-MEL28, was isolated from an axillary lymph node of a patient [40]. Involvement of the lymph nodes suggest that this melanoma has advanced to Stage III, implying that this cell line is highly malignant [41]. B16 cells were harvested from a tumor which developed naturally surrounding the ear of a C57BL/6 mouse. In this study we used the highly metastatic and aggressive variant B16.F10, which has classically been described as a non- or low-immunogenic tumor cell line [42]. No correlations were drawn between the origin of the cell line, its stage and the response to macrophage depletion, as we found that the *in situ* melanoma ZMEL1 and the highly malignant melanoma SK-MEL28 both progressed better in the

absence of macrophages, while a similar malignant melanoma B16.F10 showed impaired growth under the same circumstances. These results imply that only xenografted B16.F10 tumors profit from macrophages during development. Considering that B16.F10 is a low-immunogenic cell line, we decided not to focus on the immunosuppressive function of macrophages, but on their ability to promote angiogenesis.

To assess the importance of macrophages in tumor-induced angiogenesis, we firstly proved that ZMEL1 and B16.F10 cells were able to form a solid tumor with neo-vascularization. Macrophage depletion severely impaired the neo-vascularization of the B16.F10 tumor. In previous research, it was found that the presence of pro-inflammatory macrophages leads to a significant increase in the amount and complexity of blood vessels. Pro-inflammatory macrophages, which can act as a local source of VEGF, are often associated with the vessel tips, thereby inducing vessel sprouting. Another mechanism by which macrophages support angiogenesis is through dislodging neutrophils from the vessel tips. Neutrophils were found to exhibit inhibitory angiogenic influences, and therefore require dislodging to promote angiogenesis [43]. Possibly, due to macrophage ablation, the angiogenic switch of the B16.F10 tumor is tilted towards an anti-angiogenic outcome, resulting in severely impaired tumor vascularization, which in turn inhibited tumor growth [44]. In contrast, ZMEL1 neo-angiogenesis was not affected by macrophage depletion. The ability of ZMEL1 to produce zebrafish VEGFA could explain why this tumor is capable of inducing angiogenesis in the absence of macrophages. Possibly, ZMEL1 tumors rely on their own production of VEGFA to tilt the angiogenic switch to a pro-angiogenic outcome. To strengthen this hypothesis, we assessed the ability of tumor cells to induce sprouting or attract blood vessels from the SIV. Consistent with our previous findings, B16.F10 showed the highest angiogenic activity. Ablation of macrophages impaired this activity, whereas ZMEL1 induced angiogenesis was not affected. These results strongly imply that the mechanism behind vascularization varies between each cell line. However, we found that cell lines which rely on macrophages for angiogenesis, also showed impaired growth in the absence of macrophages at 6dpi.

In the end, we used zebrafish macrophages attraction assays to prove that lactic acid function as chemoattractant to recruit macrophages comparing to well-known cytokine, hCCL2. After chemical inhibition of glycolysis hence lactic acid secretion, less macrophages were attracted to the tumor site and tumor angiogenesis was impaired. Surprisingly the tumor burden at 2dpi was not significantly influenced by 2DG treatment presumably due to a short duration of the experiment. In future, genetic interference approach is required to further prove that angiogenesis induction by high glycolytic cells is indeed control by lactic acid dependent macrophages attraction.

In summary, our findings demonstrate that macrophages can promote melanoma growth by inducing angiogenesis in the zebrafish xenograft model. Our results show that there is no universal mechanism

by which melanoma cell lines induce and rely on angiogenesis, but that this is cell line specific. We found that the growth of melanoma, which is able to induce angiogenesis in the absence of macrophages, was not promoted by macrophages. Similarly, macrophages did not promote growth of melanoma which did not induce neo-angiogenesis. Importantly, we found that macrophages are attracted by lactic acid to promote tumor angiogenesis in B16.F10 cells.

In conclusion, this study has aided in the understanding of the interactions between macrophages and melanoma cells, and serves as a foundation for further research aimed to discover the exact mechanism by which macrophages induce neo-angiogenesis in melanoma with high glycolytic index.

## Reference

1. Ossio, R.; Roldán-Marín, R.; Martínez-Said, H.; Adams, D.J.; Robles-Espinoza, C.D. Melanoma: a global perspective. *Nat Rev Cancer* **2017**, *17*, 393-394, doi:10.1038/nrc.2017.43.
2. Leonardi, G.C.; Falzone, L.; Salemi, R.; Zanghi, A.; Spandidos, D.A.; McCubrey, J.A.; Candido, S.; Libra, M. Cutaneous melanoma: From pathogenesis to therapy (Review). *Int J Oncol* **2018**, *52*, 1071-1080, doi:10.3892/ijo.2018.4287.
3. Prasad, C.P.; Mohapatra, P.; Andersson, T. Therapy for BRAFi-Resistant Melanomas: Is WNT5A the Answer? *Cancers* **2015**, *7*, 1900-1924, doi:10.3390/cancers7030868.
4. Nishida, N.; Yano, H.; Nishida, T.; Kamura, T.; Kojiro, M. Angiogenesis in cancer. *Vascular health and risk management* **2006**, *2*, 213-219, doi:10.2147/vhrm.2006.2.3.213.
5. Sceneay, J.; Smyth, M.J.; Möller, A. The pre-metastatic niche: finding common ground. *Cancer metastasis reviews* **2013**, *32*, 449-464, doi:10.1007/s10555-013-9420-1.
6. Maman, S.; Witz, I.P. A history of exploring cancer in context. *Nat Rev Cancer* **2018**, *18*, 359-376, doi:10.1038/s41568-018-0006-7.
7. Gajewski, T.F.; Schreiber, H.; Fu, Y.X. Innate and adaptive immune cells in the tumor microenvironment. *Nature immunology* **2013**, *14*, 1014-1022, doi:10.1038/ni.2703.
8. Criscitiello, C. Tumor-associated antigens in breast cancer. *Breast care (Basel, Switzerland)* **2012**, *7*, 262-266, doi:10.1159/000342164.
9. Kroemer, G.; Senovilla, L.; Galluzzi, L.; André, F.; Zitvogel, L. Natural and therapy-induced immunosurveillance in breast cancer. *Nature medicine* **2015**, *21*, 1128-1138, doi:10.1038/nm.3944.
10. Gao, F.; Liang, B.; Reddy, S.T.; Farias-Eisner, R.; Su, X. Role of inflammation-associated microenvironment in tumorigenesis and metastasis. *Current cancer drug targets* **2014**, *14*, 30-45, doi:10.2174/15680096113136660107.
11. Criscitiello, C.; Esposito, A.; Curigliano, G. Tumor-stroma crosstalk: targeting stroma in breast cancer. *Current opinion in oncology* **2014**, *26*, 551-555, doi:10.1097/cco.000000000000122.
12. Arnold, K.M.; Opdenaker, L.M.; Flynn, D.; Sims-Mourtada, J. Wound healing and cancer stem cells: inflammation as a driver of treatment resistance in breast cancer. *Cancer growth and metastasis* **2015**, *8*, 1-13, doi:10.4137/cgm.s11286.
13. Gazzaniga, S.; Bravo, A.I.; Guglielmotti, A.; van Rooijen, N.; Maschi, F.; Vecchi, A.; Mantovani, A.; Mordoh, J.; Wainstok, R. Targeting tumor-associated macrophages and inhibition of MCP-1 reduce angiogenesis and tumor growth in a human melanoma xenograft. *The Journal of investigative dermatology* **2007**, *127*, 2031-2041, doi:10.1038/sj.jid.5700827.
14. Das, A.; Sinha, M.; Datta, S.; Abas, M.; Chaffee, S.; Sen, C.K.; Roy, S. Monocyte and macrophage plasticity in tissue repair and regeneration. *The American journal of pathology* **2015**, *185*, 2596-2606, doi:10.1016/j.ajpath.2015.06.001.
15. Williams, C.B.; Yeh, E.S.; Soloff, A.C. Tumor-associated macrophages: unwitting accomplices in breast cancer malignancy. *NPJ breast cancer* **2016**, *2*, 15025-, doi:10.1038/npjbcancer.2015.25.
16. Biswas, S.K.; Mantovani, A. Macrophage plasticity and interaction with lymphocyte subsets: cancer as a paradigm. *Nature immunology* **2010**, *11*, 889-896, doi:10.1038/ni.1937.
17. Geeraerts, X.; Bolli, E.; Fendt, S.M.; Van Ginderachter, J.A. Macrophage Metabolism As Therapeutic Target for Cancer, Atherosclerosis, and Obesity. *Frontiers in immunology* **2017**,

- 8, 289, doi:10.3389/fimmu.2017.00289.
18. Mantovani, A.; Sica, A. Macrophages, innate immunity and cancer: balance, tolerance, and diversity. *Current opinion in immunology* **2010**, *22*, 231-237, doi:10.1016/j.coi.2010.01.009.
  19. Ohtsuki, T.; Kimura, K.; Tokunaga, Y.; Tsukiyama-Kohara, K.; Tateno, C.; Hayashi, Y.; Hishima, T.; Kohara, M. M2 Macrophages Play Critical Roles in Progression of Inflammatory Liver Disease in Hepatitis C Virus Transgenic Mice. *Journal of virology* **2016**, *90*, 300-307, doi:10.1128/jvi.02293-15.
  20. Hao, N.B.; Lü, M.H.; Fan, Y.H.; Cao, Y.L.; Zhang, Z.R.; Yang, S.M. Macrophages in tumor microenvironments and the progression of tumors. *Clinical & developmental immunology* **2012**, *2012*, 948098, doi:10.1155/2012/948098.
  21. Panni, R.Z.; Linehan, D.C.; DeNardo, D.G. Targeting tumor-infiltrating macrophages to combat cancer. *Immunotherapy* **2013**, *5*, 1075-1087, doi:10.2217/imt.13.102.
  22. Hussein, M.R. Tumour-associated macrophages and melanoma tumourigenesis: integrating the complexity. *International journal of experimental pathology* **2006**, *87*, 163-176, doi:10.1111/j.1365-2613.2006.00478.x.
  23. Torisu, H.; Ono, M.; Kiryu, H.; Furue, M.; Ohmoto, Y.; Nakayama, J.; Nishioka, Y.; Sone, S.; Kuwano, M. Macrophage infiltration correlates with tumor stage and angiogenesis in human malignant melanoma: possible involvement of TNFalpha and IL-1alpha. *International journal of cancer* **2000**, *85*, 182-188.
  24. Howe, K.; Clark, M.D.; Torroja, C.F.; Torrance, J.; Berthelot, C.; Muffato, M.; Collins, J.E.; Humphray, S.; McLaren, K.; Matthews, L., et al. The zebrafish reference genome sequence and its relationship to the human genome. *Nature* **2013**, *496*, 498-503, doi:10.1038/nature12111.
  25. Zhao, S.; Huang, J.; Ye, J. A fresh look at zebrafish from the perspective of cancer research. *Journal of experimental & clinical cancer research : CR* **2015**, *34*, 80, doi:10.1186/s13046-015-0196-8.
  26. Ellett, F.; Lieschke, G.J. Zebrafish as a model for vertebrate hematopoiesis. *Current opinion in pharmacology* **2010**, *10*, 563-570, doi:10.1016/j.coph.2010.05.004.
  27. Mesureur, J.; Feliciano, J.R.; Wagner, N.; Gomes, M.C.; Zhang, L.; Blanco-Gonzalez, M.; van der Vaart, M.; O'Callaghan, D.; Meijer, A.H.; Vergunst, A.C. Macrophages, but not neutrophils, are critical for proliferation of *Burkholderia cenocepacia* and ensuing host-damaging inflammation. *PLoS Pathog* **2017**, *13*, e1006437-e1006437, doi:10.1371/journal.ppat.1006437.
  28. Heilmann, S.; Ratnakumar, K.; Langdon, E.; Kansler, E.; Kim, I.; Campbell, N.R.; Perry, E.; McMahon, A.; Kaufman, C.; van Rooijen, E., et al. A Quantitative System for Studying Metastasis Using Transparent Zebrafish. *Cancer Res* **2015**, *75*, 4272-4282, doi:10.1158/0008-5472.can-14-3319.
  29. Chen, Q.; Ramu, V.; Aydar, Y.; Groenewoud, A.; Zhou, X.Q.; Jager, M.J.; Cole, H.; Cameron, C.G.; McFarland, S.A.; Bonnet, S., et al. TLD1433 Photosensitizer Inhibits Conjunctival Melanoma Cells in Zebrafish Ectopic and Orthotopic Tumour Models. *Cancers* **2020**, *12*, doi:10.3390/cancers12030587.
  30. He, S.; Lamers, G.E.; Beenakker, J.W.; Cui, C.; Ghotra, V.P.; Danen, E.H.; Meijer, A.H.; Spaink, H.P.; Snaar-Jagalska, B.E. Neutrophil-mediated experimental metastasis is enhanced by VEGFR inhibition in a zebrafish xenograft model. *J Pathol* **2012**, *227*, 431-445, doi:10.1002/path.4013.
  31. Nicoli, S.; Presta, M. The zebrafish/tumor xenograft angiogenesis assay. *Nature protocols* **2007**, *2*, 2918-2923, doi:10.1038/nprot.2007.412.
  32. Li, Y.J.; Hu, B. Establishment of multi-site infection model in zebrafish larvae for studying *Staphylococcus aureus* infectious disease. *Journal of genetics and genomics = Yi chuan xue bao* **2012**, *39*, 521-534, doi:10.1016/j.jgg.2012.07.006.
  33. Ellett, F.; Pase, L.; Hayman, J.W.; Andrianopoulos, A.; Lieschke, G.J. mpeg1 promoter transgenes direct macrophage-lineage expression in zebrafish. *Blood* **2011**, *117*, e49-56, doi:10.1182/blood-2010-10-314120.
  34. Gray, C.; Loynes, C.A.; Whyte, M.K.; Crossman, D.C.; Renshaw, S.A.; Chico, T.J. Simultaneous intravital imaging of macrophage and neutrophil behaviour during inflammation using a novel transgenic zebrafish. *Thrombosis and haemostasis* **2011**, *105*, 811-819, doi:10.1160/th10-08-0525.

35. Colegio, O.R.; Chu, N.Q.; Szabo, A.L.; Chu, T.; Rhebergen, A.M.; Jairam, V.; Cyrus, N.; Brokowski, C.E.; Eisenbarth, S.C.; Phillips, G.M., et al. Functional polarization of tumour-associated macrophages by tumour-derived lactic acid. *Nature* **2014**, *513*, 559-563, doi:10.1038/nature13490.
36. Cambier, C.J.; Takaki, K.K.; Larson, R.P.; Hernandez, R.E.; Tobin, D.M.; Urdahl, K.B.; Cosma, C.L.; Ramakrishnan, L. Mycobacteria manipulate macrophage recruitment through coordinated use of membrane lipids. *Nature* **2014**, *505*, 218-222, doi:10.1038/nature12799.
37. Dvorak, H.F. Tumors: wounds that do not heal-redux. *Cancer immunology research* **2015**, *3*, 1-11, doi:10.1158/2326-6066.cir-14-0209.
38. Heilmann, S.; Ratnakumar, K.; Langdon, E.; Kansler, E.; Kim, I.; Campbell, N.R.; Perry, E.; McMahon, A.; Kaufman, C.; van Rooijen, E., et al. A Quantitative System for Studying Metastasis Using Transparent Zebrafish. *Cancer Res* **2015**, *75*, 4272-4282, doi:10.1158/0008-5472.CAN-14-3319.
39. Kansler, E.R.; Verma, A.; Langdon, E.M.; Simon-Vermot, T.; Yin, A.; Lee, W.; Attiyeh, M.; Elemento, O.; White, R.M. Melanoma genome evolution across species. *BMC Genomics* **2017**, *18*, 136-136, doi:10.1186/s12864-017-3518-8.
40. Carey, T.E.; Takahashi, T.; Resnick, L.A.; Oettgen, H.F.; Old, L.J. Cell surface antigens of human malignant melanoma: mixed hemadsorption assays for humoral immunity to cultured autologous melanoma cells. *Proceedings of the National Academy of Sciences of the United States of America* **1976**, *73*, 3278-3282, doi:10.1073/pnas.73.9.3278.
41. Bevilacqua, R.G.; Coit, D.G.; Rogatko, A.; Younes, R.N.; Brennan, M.F. Axillary dissection in melanoma. Prognostic variables in node-positive patients. *Annals of surgery* **1990**, *212*, 125-131, doi:10.1097/0000658-199008000-00002.
42. Overwijk, W.W.; Restifo, N.P. B16 as a mouse model for human melanoma. *Current protocols in immunology* **2001**, *Chapter 20*, Unit 20.21, doi:10.1002/0471142735.im2001s39.
43. Gurevich, D.B.; Severn, C.E.; Twomey, C.; Greenhough, A.; Cash, J.; Toye, A.M.; Mellor, H.; Martin, P. Live imaging of wound angiogenesis reveals macrophage orchestrated vessel sprouting and regression. *The EMBO journal* **2018**, *37*, doi:10.15252/embj.201797786.
44. Baeriswyl, V.; Christofori, G. The angiogenic switch in carcinogenesis. *Seminars in cancer biology* **2009**, *19*, 329-337, doi:10.1016/j.semcancer.2009.05.003.
45. Wong, J.R.; Nanji, A.A.; Galor, A.; Karp, C.L. Management of conjunctival malignant melanoma: a review and update. *Expert Rev Ophthalmol* **2014**, *9*, 185-204, doi:10.1586/17469899.2014.921119.
46. Eskandarpour, M.; Huang, F.; Reeves, K.A.; Clark, E.; Hansson, J. Oncogenic NRAS has multiple effects on the malignant phenotype of human melanoma cells cultured in vitro. *Int J Cancer* **2009**, *124*, 16-26, doi:10.1002/ijc.23876.
47. Larsen, A.C. Conjunctival malignant melanoma in Denmark: epidemiology, treatment and prognosis with special emphasis on tumorigenesis and genetic profile. *Acta ophthalmologica* **2016**, *94 Thesis 1*, 1-27, doi:10.1111/aos.13100.
48. Missotten, G.S.; Keijser, S.; De Keizer, R.J.; De Wolff-Rouendaal, D. Conjunctival melanoma in the Netherlands: a nationwide study. *Invest Ophthalmol Vis Sci* **2005**, *46*, 75-82, doi:10.1167/iovs.04-0344.
49. Brouwer, N.J.; Marinkovic, M.; van Duinen, S.G.; Bleeker, J.C.; Jager, M.J.; Luyten, G.P.M. Treatment of conjunctival melanoma in a Dutch referral centre. *The British journal of ophthalmology* **2018**, *102*, 1277-1282, doi:10.1136/bjophthalmol-2017-311082.
50. Esmaeli, B.; Rubin, M.L.; Xu, S.; Goepfert, R.P.; Curry, J.L.; Prieto, V.G.; Ning, J.; Tetzlaff, M.T. Greater Tumor Thickness, Ulceration, and Positive Sentinel Lymph Node Are Associated With Worse Prognosis in Patients With Conjunctival Melanoma: Implications for Future AJCC Classifications. *The American journal of surgical pathology* **2019**, *43*, 1701-1710, doi:10.1097/pas.0000000000001344.
51. Cao, J.; Heijkants, R.C.; Jochemsen, A.G.; Dogrusoz, M.; de Lange, M.J.; van der Velden, P.A.; van der Burg, S.H.; Jager, M.J.; Verdijk, R.M. Targeting of the MAPK and AKT pathways in conjunctival melanoma shows potential synergy. *Oncotarget* **2017**, *8*, 58021-58036, doi:10.18632/oncotarget.10770.
52. Griewank, K.G.; Westekemper, H.; Murali, R.; Mach, M.; Schilling, B.; Wiesner, T.; Schimming, T.; Livingstone, E.; Sucker, A.; Grabellus, F., et al. Conjunctival melanomas harbor BRAF and NRAS mutations and copy number changes similar to cutaneous and mucosal melanomas.

- Clin Cancer Res* **2013**, *19*, 3143-3152, doi:10.1158/1078-0432.ccr-13-0163.
53. Larsen, A.C.; Dahmcke, C.M.; Dahl, C.; Siersma, V.D.; Toft, P.B.; Coupland, S.E.; Prause, J.U.; Guldberg, P.; Heegaard, S. A Retrospective Review of Conjunctival Melanoma Presentation, Treatment, and Outcome and an Investigation of Features Associated With BRAF Mutations. *JAMA ophthalmology* **2015**, *133*, 1295-1303, doi:10.1001/jamaophthalmol.2015.3200.
  54. Cao, J.; Pontes, K.C.; Heijkants, R.C.; Brouwer, N.J.; Groenewoud, A.; Jordanova, E.S.; Marinkovic, M.; van Duinen, S.; Teunisse, A.F.; Verdijk, R.M., et al. Overexpression of EZH2 in conjunctival melanoma offers a new therapeutic target. *J Pathol* **2018**, *245*, 433-444, doi:10.1002/path.5094.
  55. Pontes, K.C.S.; Groenewoud, A.; Cao, J.; Ataide, L.M.S.; Snaar-Jagalska, E.; Jager, M.J. Evaluation of (fli:GFP) Casper Zebrafish Embryos as a Model for Human Conjunctival Melanoma. *Invest Ophthalmol Vis Sci* **2017**, *58*, 6065-6071, doi:10.1167/iovs.17-22023.
  56. Banerji, U.; Affolter, A.; Judson, I.; Marais, R.; Workman, P. BRAF and NRAS mutations in melanoma: potential relationships to clinical response to HSP90 inhibitors. *Molecular cancer therapeutics* **2008**, *7*, 737-739, doi:10.1158/1535-7163.mct-08-0145.
  57. McCain, J. The MAPK (ERK) Pathway: Investigational Combinations for the Treatment Of BRAF-Mutated Metastatic Melanoma. *P & T: a peer-reviewed journal for formulary management* **2013**, *38*, 96-108.
  58. Scholz, S.L.; Cosgarea, I.; Susskind, D.; Murali, R.; Moller, I.; Reis, H.; Leonardelli, S.; Schilling, B.; Schimming, T.; Hadaschik, E., et al. NF1 mutations in conjunctival melanoma. *Br J Cancer* **2018**, *118*, 1243-1247, doi:10.1038/s41416-018-0046-5.
  59. Dos Santos, A.I.F.; De Almeida, D.R.Q.; Terra, L.F.; Baptista, M.c.S.; Labriola, L. Photodynamic therapy in cancer treatment - an update review. *Journal of Cancer Metastasis and Treatment* **2019**, *2019*, doi:10.20517/2394-4722.2018.83.
  60. Triesscheijn, M.; Baas, P.; Schellens, J.H.; Stewart, F.A. Photodynamic therapy in oncology. *Oncologist* **2006**, *11*, 1034-1044, doi:10.1634/theoncologist.11-9-1034.
  61. Dolmans, D.E.; Fukumura, D.; Jain, R.K. Photodynamic therapy for cancer. *Nature reviews. Cancer* **2003**, *3*, 380-387, doi:10.1038/nrc1071.
  62. Frochot, C.; Mordon, S. Update of the situation of clinical photodynamic therapy in Europe in the 2003–2018 period. *Journal of Porphyrins and Phthalocyanines* **2019**, *23*, 347-357, doi:10.1142/s1088424619300027.
  63. Monro, S.; Colón, K.L.; Yin, H.; Roque, J.; Konda, P.; Gujar, S.; Thummel, R.P.; Lilge, L.; Cameron, C.G.; McFarland, S.A. Transition Metal Complexes and Photodynamic Therapy from a Tumor-Centered Approach: Challenges, Opportunities, and Highlights from the Development of TLD1433. *Chemical Reviews* **2019**, *119*, 797-828, doi:10.1021/acs.chemrev.8b00211.
  64. Chibazakura, T.; Toriyabe, Y.; Fujii, H.; Takahashi, K.; Kawakami, M.; Kuwamura, H.; Haga, H.; Ogura, S.; Abe, F.; Nakajima, M., et al. 5-Aminolevulinic acid enhances cell death under thermal stress in certain cancer cell lines. *Bioscience, biotechnology, and biochemistry* **2015**, *79*, 422-431, doi:10.1080/09168451.2014.975186.
  65. Kennedy, J.C.; Pottier, R.H.; Pross, D.C. Photodynamic therapy with endogenous protoporphyrin IX: basic principles and present clinical experience. *Journal of photochemistry and photobiology. B, Biology* **1990**, *6*, 143-148, doi:10.1016/1011-1344(90)85083-9.
  66. Kaspler, P.; Lazic, S.; Forward, S.; Arenas, Y.; Mandel, A.; Lilge, L. A ruthenium(ii) based photosensitizer and transferrin complexes enhance photo-physical properties, cell uptake, and photodynamic therapy safety and efficacy. *Photochemical & photobiological sciences: Official journal of the European Photochemistry Association and the European Society for Photobiology* **2016**, *15*, 481-495, doi:10.1039/c5pp00450k.
  67. Molpus, K.L.; Kato, D.; Hamblin, M.R.; Lilge, L.; Bamberg, M.; Hasan, T. Intraperitoneal photodynamic therapy of human epithelial ovarian carcinomatosis in a xenograft murine model. *Cancer Res* **1996**, *56*, 1075-1082.
  68. Elliott, J.T.; Samkoe, K.S.; Gunn, J.R.; Stewart, E.E.; Gardner, T.B.; Tichauer, K.M.; Lee, T.Y.; Hoopes, P.J.; Pereira, S.P.; Hasan, T., et al. Perfusion CT estimates photosensitizer uptake and biodistribution in a rabbit orthotopic pancreatic cancer model: a pilot study. *Academic radiology* **2015**, *22*, 572-579, doi:10.1016/j.acra.2014.12.014.
  69. Engbrecht, B.W.; Menon, C.; Kachur, A.V.; Hahn, S.M.; Fraker, D.L. Photofrin-mediated photodynamic therapy induces vascular occlusion and apoptosis in a human sarcoma

- xenograft model. *Cancer Res* **1999**, *59*, 4334-4342.
70. McFarland, S.A.; Mandel, A.; Dumoulin-White, R.; Gasser, G. Metal-based photosensitizers for photodynamic therapy: the future of multimodal oncology? *Curr Opin Chem Biol* **2019**, *56*, 23-27, doi:10.1016/j.cbpa.2019.10.004.
  71. Ramu, V.; Aute, S.; Taye, N.; Guha, R.; Walker, M.G.; Mogare, D.; Parulekar, A.; Thomas, J.A.; Chattopadhyay, S.; Das, A. Photo-induced cytotoxicity and anti-metastatic activity of ruthenium(ii)-polypyridyl complexes functionalized with tyrosine or tryptophan. *Dalton transactions (Cambridge, England : 2003)* **2017**, *46*, 6634-6644, doi:10.1039/c7dt00670e.
  72. Heinemann, F.; Karges, J.; Gasser, G. Critical Overview of the Use of Ru(II) Polypyridyl Complexes as Photosensitizers in One-Photon and Two-Photon Photodynamic Therapy. *Accounts of chemical research* **2017**, *50*, 2727-2736, doi:10.1021/acs.accounts.7b00180.
  73. Fong, J.; Kasimova, K.; Arenas, Y.; Kaspler, P.; Lazic, S.; Mandel, A.; Lilge, L. A novel class of ruthenium-based photosensitizers effectively kills in vitro cancer cells and in vivo tumors. *Photochemical & photobiological sciences : Official journal of the European Photochemistry Association and the European Society for Photobiology* **2015**, *14*, 2014-2023, doi:10.1039/c4pp00438h.
  74. Liu, S.; Leach, S.D. Zebrafish models for cancer. *Annual review of pathology* **2011**, *6*, 71-93, doi:10.1146/annurev-pathol-011110-130330.
  75. Goessling, W.; North, T.E.; Zon, L.I. New waves of discovery: modeling cancer in zebrafish. *Journal of clinical oncology : official journal of the American Society of Clinical Oncology* **2007**, *25*, 2473-2479, doi:10.1200/jco.2006.08.9821.
  76. Howe, K.; Clark, M.D.; Torroja, C.F.; Torrance, J.; Berthelot, C.; Muffato, M.; Collins, J.E.; Humphray, S.; McLaren, K.; Matthews, L., et al. The zebrafish reference genome sequence and its relationship to the human genome. *Nature* **2013**, *496*, 498-503, doi:10.1038/nature12111.
  77. Amatruda, J.F.; Shepard, J.L.; Stern, H.M.; Zon, L.I. Zebrafish as a cancer model system. *Cancer cell* **2002**, *1*, 229-231, doi:10.1016/s1535-6108(02)00052-1.
  78. Lam, S.H.; Chua, H.L.; Gong, Z.; Lam, T.J.; Sin, Y.M. Development and maturation of the immune system in zebrafish, *Danio rerio*: a gene expression profiling, in situ hybridization and immunological study. *Developmental and comparative immunology* **2004**, *28*, 9-28, doi:10.1016/s0145-305x(03)00103-4.
  79. Zon, L.I.; Peterson, R.T. In vivo drug discovery in the zebrafish. *Nature reviews. Drug discovery* **2005**, *4*, 35-44, doi:10.1038/nrd1606.
  80. Lawson, N.D.; Weinstein, B.M. In vivo imaging of embryonic vascular development using transgenic zebrafish. *Dev Biol* **2002**, *248*, 307-318, doi:10.1006/dbio.2002.0711.
  81. Renshaw, S.A.; Loynes, C.A.; Trushell, D.M.; Elworthy, S.; Ingham, P.W.; Whyte, M.K. A transgenic zebrafish model of neutrophilic inflammation. *Blood* **2006**, *108*, 3976-3978, doi:10.1182/blood-2006-05-024075.
  82. Manghnani, P.N.; Wu, W.; Xu, S.; Hu, F.; Teh, C.; Liu, B. Visualizing Photodynamic Therapy in Transgenic Zebrafish Using Organic Nanoparticles with Aggregation-Induced Emission. *Nano-micro letters* **2018**, *10*, 61, doi:10.1007/s40820-018-0214-4.
  83. Wang, C.; Qian, Y. A water soluble carbazolyl-BODIPY photosensitizer with an orthogonal D-A structure for photodynamic therapy in living cells and zebrafish. *Biomaterials science* **2019**, *10.1039/c9bm01709g*, doi:10.1039/c9bm01709g.
  84. Hanson, K.; Robinson, S.D.; Al-Yousuf, K.; Hendry, A.E.; Sexton, D.W.; Sherwood, V.; Wheeler, G.N. The anti-rheumatic drug, leflunomide, synergizes with MEK inhibition to suppress melanoma growth. *Oncotarget* **2018**, *9*, 3815-3829, doi:10.18632/oncotarget.23378.
  85. van der Ent, W.; Burrello, C.; Teunisse, A.F.; Ksander, B.R.; van der Velden, P.A.; Jager, M.J.; Jochemsen, A.G.; Snaar-Jagalska, B.E. Modeling of human uveal melanoma in zebrafish xenograft embryos. *Investigative ophthalmology & visual science* **2014**, *55*, 6612-6622, doi:10.1167/iovs.14-15202.
  86. Chapman, A.; Fernandez del Ama, L.; Ferguson, J.; Kamarashev, J.; Wellbrock, C.; Hurlstone, A. Heterogeneous tumor subpopulations cooperate to drive invasion. *Cell Rep* **2014**, *8*, 688-695, doi:10.1016/j.celrep.2014.06.045.
  87. Nicoli, S.; Ribatti, D.; Cotelli, F.; Presta, M. Mammalian tumor xenografts induce neovascularization in zebrafish embryos. *Cancer Res* **2007**, *67*, 2927-2931, doi:10.1158/0008-5472.CAN-06-4268.

88. Wang, J.; Cao, Z.; Zhang, X.M.; Nakamura, M.; Sun, M.; Hartman, J.; Harris, R.A.; Sun, Y.; Cao, Y. Novel mechanism of macrophage-mediated metastasis revealed in a zebrafish model of tumor development. *Cancer Res* **2015**, *75*, 306-315, doi:10.1158/0008-5472.CAN-14-2819.
89. Wehmas, L.C.; Tanguay, R.L.; Punnoose, A.; Greenwood, J.A. Developing a Novel Embryo-Larval Zebrafish Xenograft Assay to Prioritize Human Glioblastoma Therapeutics. *Zebrafish* **2016**, *13*, 317-329, doi:10.1089/zeb.2015.1170.
90. Nareyeck, G.; Wuestemeyer, H.; von der Haar, D.; Anastassiou, G. Establishment of two cell lines derived from conjunctival melanomas. *Experimental eye research* **2005**, *81*, 361-362, doi:10.1016/j.exer.2005.04.018.
91. Keijser, S.; Maat, W.; Missotten, G.S.; de Keizer, R.J. A new cell line from a recurrent conjunctival melanoma. *The British journal of ophthalmology* **2007**, *91*, 1566-1567, doi:10.1136/bjo.2006.110841.
92. Luyten, G.P.; Naus, N.C.; Mooy, C.M.; Hagemeyer, A.; Kan-Mitchell, J.; Van Drunen, E.; Vuzevski, V.; De Jong, P.T.; Luider, T.M. Establishment and characterization of primary and metastatic uveal melanoma cell lines. *International journal of cancer* **1996**, *66*, 380-387, doi:10.1002/(sici)1097-0215(19960503)66:3<380::aid-ijc19>3.0.co;2-f.
93. Chen, P.W.; Murray, T.G.; Uno, T.; Salgaller, M.L.; Reddy, R.; Ksander, B.R. Expression of MAGE genes in ocular melanoma during progression from primary to metastatic disease. *Clinical & experimental metastasis* **1997**, *15*, 509-518, doi:10.1023/a:1018479011340.
94. Carlotti, F.; Bazuine, M.; Kekarainen, T.; Seppen, J.; Pognonec, P.; Maassen, J.A.; Hoeben, R.C. Lentiviral vectors efficiently transduce quiescent mature 3T3-L1 adipocytes. *Molecular therapy : the journal of the American Society of Gene Therapy* **2004**, *9*, 209-217, doi:10.1016/j.ymthe.2003.11.021.
95. Hopkins, S.L.; Siewert, B.; Askes, S.H.; Veldhuizen, P.; Zwier, R.; Heger, M.; Bonnet, S. An in vitro cell irradiation protocol for testing photopharmaceuticals and the effect of blue, green, and red light on human cancer cell lines. *Photochemical & photobiological sciences : Official journal of the European Photochemistry Association and the European Society for Photobiology* **2016**, *15*, 644-653, doi:10.1039/c5pp00424a.
96. Hopkins, S.L.; Siewert, B.; Askes, S.H.C.; Veldhuizen, P.; Zwier, R.; Heger, M.; Bonnet, S. An in vitro cell irradiation protocol for testing photopharmaceuticals and the effect of blue, green, and red light on human cancer cell lines. *Photochemical & photobiological sciences : Official journal of the European Photochemistry Association and the European Society for Photobiology* **2016**, *15*, 644-653, doi:10.1039/c5pp00424a.
97. Cuello-Garibo, J.-A.; Meijer, M.S.; Bonnet, S. To cage or to be caged? The cytotoxic species in ruthenium-based photoactivated chemotherapy is not always the metal. *Chem Commun (Camb)* **2017**, *53*, 6768-6771, doi:10.1039/c7cc03469e.
98. Monro, S.; Colón, K.L.; Yin, H.; Roque, J., 3rd; Konda, P.; Gujar, S.; Thummel, R.P.; Lilge, L.; Cameron, C.G.; McFarland, S.A. Transition Metal Complexes and Photodynamic Therapy from a Tumor-Centered Approach: Challenges, Opportunities, and Highlights from the Development of TLD1433. *Chemical reviews* **2019**, *119*, 797-828, doi:10.1021/acs.chemrev.8b00211.
99. Galluzzi, L.; Vitale, I.; Aaronson, S.A.; Abrams, J.M.; Adam, D.; Agostinis, P.; Alnemri, E.S.; Altucci, L.; Amelio, I.; Andrews, D.W., et al. Molecular mechanisms of cell death: recommendations of the Nomenclature Committee on Cell Death 2018. *Cell Death Differ* **2018**, *25*, 486-541, doi:10.1038/s41418-017-0012-4.
100. Mishra, R.R.; Kneitz, S.; Scharl, M. Comparative analysis of melanoma deregulated miRNAs in the medaka and Xiphophorus pigment cell cancer models. *Comparative biochemistry and physiology. Toxicology & pharmacology : CBP* **2014**, *163*, 64-76, doi:10.1016/j.cbpc.2014.01.002.
101. Li, H.; Qian, Z.M. Transferrin/transferrin receptor-mediated drug delivery. *Medicinal research reviews* **2002**, *22*, 225-250, doi:10.1002/med.10008.
102. Qian, Z.M.; Li, H.; Sun, H.; Ho, K. Targeted drug delivery via the transferrin receptor-mediated endocytosis pathway. *Pharmacological reviews* **2002**, *54*, 561-587, doi:10.1124/pr.54.4.561.
103. Johnsen, K.B.; Burkhart, A.; Thomsen, L.B.; Andresen, T.L.; Moos, T. Targeting the transferrin receptor for brain drug delivery. *Progress in neurobiology* **2019**, *181*, 101665, doi:10.1016/j.pneurobio.2019.101665.